Available online at www.sciencedirect.com
SCIENCE DIRECT®
Combustion and Flame 136 (2004) 25–42
Combustion and Flame
www.elsevier.com/locate/jnlabr/cnf

Shock-tube study of methane ignition under engine-relevant conditions: experiments and modeling

J. Huang,[a,*] P.G. Hill,[a] W.K. Bushe,[a] and S.R. Munshi [b]

[a] *Department of Mechanical Engineering, University of British Columbia, Vancouver, BC, Canada V6T 1Z4*
[b] *Westport Innovations Inc., Vancouver, BC, Canada*

Received 5 September 2002; received in revised form 25 August 2003; accepted 6 September 2003

Abstract

A series of shock tube experiments was conducted to measure the ignition delay of homogeneous methane/air (CH_4/air) mixtures at moderate temperatures (1000 to 1350 K) and elevated pressures (16–40 atm). The equivalence ratios of the test mixtures were varied from 0.7 to 1.3 with the focus on the slightly lean-to-stoichiometric region, which is most relevant to internal combustion (IC) engine conditions. Transitions from mild to strong ignition were observed at lower temperatures with increasing pressure. An analytical study of methane oxidation under the above conditions was conducted using a detailed chemical kinetic mechanism proposed by Petersen et al. The mechanism was modified and extended in this work, based on the experimental results and literature reviews. The current model improves the agreement between the calculated ignition delay time and experimental data. Sensitivity and reaction flow analyses show that the oxidation of methyl (to form methoxy radicals) is a main rate-limiting step in pre-ignition reactions for stoichiometric methane/air mixtures at 1250 K. At lower temperatures, the activation energy decreases due to a rapid rise in the rates of reactions $CH_3 + O_2 \Leftrightarrow CH_3O_2$ and $CH_3O_2 + CH_3 \Leftrightarrow 2CH_3O$, which effectively promotes ignition. At still lower temperatures (below 1100 K), the depletion of methyl and hydroxyl radicals becomes increasingly rate-limiting and leads to a re-increase of the activation energy. Further study of chemical kinetics for methane oxidation at high pressures, particularly for fuel-lean mixtures, is suggested to improve the agreement between the model and experiments.

Keywords: Methane ignition; High pressure; Chemical kinetics

1. Introduction

The increasing popularity of natural-gas-fueled internal combustion engines [1–3] raises the importance of predicting autoignition of natural gas under various operating conditions. Early experimental measurements of the ignition delay of methane, a major component of natural gas, were mostly conducted under low-pressure (0.5–15 atm), high temperature (1200–2500 K) [4–9], and/or highly dilute conditions (with over 90% Ar) [10]. Recent experimental shock-tube studies and kinetic modeling conducted by Petersen et al. [11–13] show that the ignition delays of methane/oxygen/argon and methane/oxygen/nitrogen mixtures under high-pressure, moderate-temperature conditions with low dilution levels are considerably different from those under low-pressure, high-temperature and high-dilution-ratio conditions. Specifically, they report a significantly reduction in the activation energy for temperatures below 1300 K. Few experimental data are available for the ignition delay time of methane/air mixtures under typical, engine-relevant conditions, that is, for initial pressures above

* Corresponding author.
E-mail address: jhuang@mech.ubc.ca (J. Huang).

0010-2180/$ – see front matter
doi:10.1016/j.combustflame.2003.09.002

Table 1
Experimental conditions and empirical coefficients for the ignition delay of methane reported in the literature

	Pressure (atm)	Temperature (K)	x	y	A $s(\mathrm{cm}^3/\mathrm{mol})^{x+y}$	E_a (kcal/mol)
Seery and Bowman [4]	1.5–4	1300–1900	0.4	−1.6	7.65E − 18	51.4
Lifshitz et al. [5]	2–10	1500–2150	0.33	−1.03	3.62E − 14	46.5
Tsuboi and Wagner [6]	2–3	1200–2100	0.32	−1.02	2.50E − 15	53.0
Cheng and Oppenheim [7]	1–3	1600–2200	0.48	−1.94	1.19E − 18	46.3
Grillo and Slack [8]	1–6	1640–2150	0.33	−1.03	4.40E − 15	52.3
Petersen et al. [12,13]	40–260	>1300	−0.02	−1.20	1.26E − 14	32.7
Petersen et al. [12,13]	40–260	<1300	−0.38	−1.31	4.99E − 14	19.0

16 atm, temperatures below 1400 K, and equivalence ratios from 0.7 to 1.3.

Because the lack of experimental data in this regime has prevented development of adequate chemical kinetic mechanisms, the primary objective of the current study was to measure the ignition delay of methane under engine-relevant conditions. The resulting experimental data have been compared with the calculations using detailed chemical kinetic mechanisms (with appropriate modifications where necessary) to obtain a deeper understanding of methane oxidation/ignition under conditions relevant to practical devices such as natural-gas-fueled engines or high-pressure gas turbines.

The current experiments were conducted in a high-pressure, stainless-steel shock tube. Unlike in other experimental methods, the temperature and pressure rises behind a shock wave are virtually instantaneous; this minimizes the effects of surface reactions or processes occurring at intermediate temperatures [14]. The quiescent state of the driven gas behind the reflected shock further simplifies the situation by reducing the gasdynamic effects. These merits make the shock tube an ideal tool for the current study.

The criteria commonly used to define the onset of ignition include sudden changes in temperature (heat transfer) and pressure, a certain radical concentration, or sudden change in density of the mixture. Zhou and Karim [15] examine the different criteria numerically using a detailed reaction mechanism, and find little difference between results of using different criteria for ignition delay at low temperatures (< 1100 K), but relatively large differences at higher temperatures. They recommend criteria based on sudden changes in pressure and temperature because ignition delay times measured by such methods generally lie between the results obtained using other criteria.

Many of the early experimental results of methane/oxygen ignition delay were correlated with initial conditions using an Arrhenius-type, parametric formula given by

$$\tau = A \exp\left(\frac{E}{RT}\right)[\mathrm{O_2}]^x[\mathrm{CH_4}]^y, \tag{1}$$

where coefficients A, E, x, and y are obtained by fitting the experimental data using regression methods. Some of the values reported for these coefficients in the literature are given in Table 1 along with their experimental conditions. Extrapolating these equations to the conditions studied in this work generates a wide scatter in predicted ignition delay time. Application of these empirical equations beyond the range where they were derived (and particularly under engine-relevant conditions) is not justified.

The correlation formula shown in Eq. (1) indicates that the type of dilution gas has a negligible effect on ignition delay. Petersen et al. [12] observed no significant difference in measured ignition delay time when the dilution gas was changed from argon to nitrogen, which suggests that ignition is primarily based on CH_4/O_2 kinetics rather than on thermal effects; however, in detailed chemical kinetic mechanisms such as GRI-Mech 3.0 [16], third-body reactions involving nitrogen do possess rate coefficients different from those involving argon; meanwhile, nitrogen has a higher enhancement coefficient in pressure-dependent reactions (such as the combination CH_3 to form C_2H_6). Furthermore, the formation of some nitrocompounds under high-temperature, high-pressure conditions may also affect the ignition delay time [17,18]. In the study reported herein, air was used to best simulate IC engine conditions.

2. Experimental

A schematic of the shock tube used in the current study is given in Fig. 1. The inner diameter of the shock tube is 59 mm. The lengths of the driver and driven sections are 3.18 and 4.25 m, respectively. The shock tube has been designed and hydraulically tested to withstand a maximum pressure of 200 atm. The initial pressure in the driver section was measured with an Eclipse static pressure transducer. The initial driven pressure was measured using an Auto-Tran 851D differential pressure transducer. The incident shock velocity was measured using five flush-mounted PCB 112B11 piezoelectric pressure transducers with a minimum response time of 3 μs. The

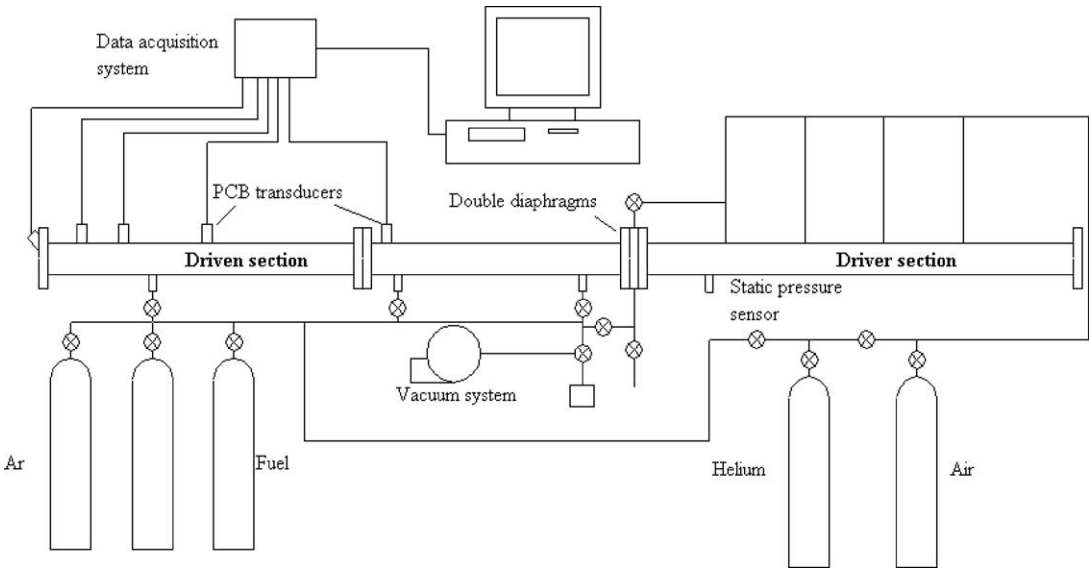

Fig. 1. Schematics of the shock tube and attached equipment.

outputs were connected to a 12-bit IOtech Wavebook-512 data acquisition system sampling at a total frequency of 1 MHz.

The temperatures and pressures behind reflected shocks were calculated by solving conservation equations across the shock front using measured incident shock velocities. The temperature-dependent thermochemical properties of the test gases were calculated using polynomial coefficients from the standard databases of GRI-Mech [16], which includes the NASA-Lewis and Technion archives [19,20]. For a driven gas with low dilution ratio (or diatomic dilution gas such as nitrogen), non-ideal shock reflection results from shock-wave/boundary-layer interactions [21–24], which lead to shock bifurcation. The temperature of the driven gas after passing the λ foot of the reflected shock and the time for the cooling flow to reach the endwall were examined using a model proposed by Mark [23] and Davies [24]. The perturbation originating from the contact surface [24] was also investigated and found to be less important given the range of ρ_5/ρ_6 (the ratio between the driven and driver pressure behind the reflected shock) in the current experiments. The uncertainty of the calculated temperature T_5 in the current study, arising from the uncertainty in the velocity measurement and non-ideal shock reflection, is around 14 K. This value agrees with the calculation based on the reflected shock speed measured at the end of the driven section using the method suggested by Skinner [25].

The location of ignition measurements reported in the literature varies from zero to several centimeters from the end plate of the driven section. Frenklach and Bornside [26] found that the ignition delay time measured at the end plate is significantly different from that measured 6.6 cm away. Petersen et al. [11] reported no noticeable difference for the results measured at 1 or 2 cm away from the end, but suggested correcting measured ignition delay data for strong ignitions if the measurement is not at the endwall [12]. For an ideal reflection, the driven gas behind the reflected shock is in a quiescent state. Heat transfer in the driven gas occurs mainly in the form of diffusion so that the thickness of the thermal layer developed from the end plate can be estimated as $d = \sqrt{\alpha t}$, where α is the thermal diffusivity and t is the time after reflection. This is a very thin layer given the shortness of the total experimental time. Fieweger et al. [27] have observed experimentally that ignitions behind reflected shocks start close to the end plate where the driven gas is exposed to the temperature behind the reflected shock from the earliest time; therefore, all ignition delays in the current study were measured using the pressure signal detected at the end plate of the driven section. This eliminates the uncertainties arising from correcting ignition data for a moving blast wave when a side-wall measurement is used [12]. The onset of ignition was defined by extrapolating the maximum rate of pressure change (dp/dt) back to the pressure right behind the reflected shock. The same method was used in many earlier studies [4,11,12].

The compositions of gas mixtures in the current study are presented in Table 2. The range of equivalence ratios (0.7–1.3) was selected to represent the most typical conditions in IC engines. The test gases—methane (99.95%) and air (99.9%; 21% O_2, 79% N_2)—were obtained from Praxair. Before each

Table 2
Test gas composition

Mixture	CH_4	Mole fractions		Φ
		O_2	N_2	
1	0.095	0.192	0.715	1
2	0.068	0.196	0.736	0.7
3	0.120	0.185	0.695	1.3

test, the driven section of the shock tube was cleaned and vacuum-pumped to an absolute pressure below 7.5×10^{-3} mbar. The vacuum was kept for about 20 min and the driven section was flushed with pure air and re-evacuated. This process removes water vapors and other possible impurities released from the wall of the shock tube at low pressures. The leakage combined with the degas rate of the driven section is below 0.25 mbar/h. The maximum uncertainty of the test-gas composition before shock heating is less than 0.2%. Methane and air were injected alternatively through three spaced ports from high-pressure storage vessels into the driven section. A 1-hr mixing time was allowed before each run to guarantee complete mixing of fuel and oxidizer. No gas mixer was used in the current experiment to avoid introducing secondary contamination from the intermediate storage vessel. To investigate the effects of finite mixing time and uncertainties in the initial mixture composition, 12 repeatability tests were conducted using mixture No. 1 at initial conditions of 40 atm and 1200 K. The residence time of the initial gas mixture in the driven section before each run was varied from 15 min to 4 hrs; four of the tests used mixtures pre-prepared in a high-pressure, stainless-steel vessel 12 hrs before the experiments. Both purified bottled air and untreated room air were used as the oxidizer for comparison (room air represents the air composition in IC engines). The standard deviation of the measured ignition delay in above tests was less than 10% without correcting for the slight difference in initial temperatures behind reflected shocks (that is, less than the relative uncertainty in temperature measurement); the maximum deviation of an individual test from the mean delay time is about 25%. These results suggest that under the conditions discussed in this work, the uncertainties resulting from the current experimental method have been controlled in an acceptable range of experimental error.

To obtain an experimental time comparable to the induction time scale in IC engines, tailored-interface conditions [14,21] were achieved in the current study by adjusting the helium/air ratio of the driver gas. The experimental time was extended to 4 to 5 ms for tailored-interface conditions, which is significantly longer than the 1-ms duration for non-tailored conditions.

3. Results and discussions

3.1. Gas dynamic features and strong ignition limit

Typical pressure histories recorded at the endwall of the shock tube are presented in Fig. 2. For temperatures between 1000 and 1200 K, methane ignition causes a mild pressure rise and a clearly distinguished pressure peak. The increase in pressure is more rapid with increasing temperature and pressure.

A noticeable change in the pressure trace occurs when the temperature is raised over a threshold between 1200 and 1300 K depending on the initial pressure. The ignition appears to be less ordered: specifically, a unique pressure maximum is no longer seen. In some cases, a sharp, secondary pressure peak—whose magnitude can exceed that of the first one—starts to appear.

With further increase in temperature, strong ignitions—characterized by sudden increases of pressure followed by violent pressure oscillations—are found. The peak pressure of a strong ignition can be 1.5 to 2 times higher than that of a mild ignition. In extreme cases, the high velocity blast wave formed in the ignition can catch up with the reflected shock and form a detonation front.

The transition from weak to strong ignition happens within a short temperature range that is pressure dependent. There is no obvious variation in the magnitude of peak pressures as the temperature approaches the strong ignition limit. Similar observation of this rapid transition for various fuels was reported in the literature [7,27–29]. Fieweger et al. [27] showed that the mild ignition observed at low temperatures originates from one or more hot spots in the experimental area and proceeds heterogeneously. In a homogeneously charged engine, mild ignitions, which evolve primarily into deflagrations, cause only moderate pressure rises and thus do not pose a threat

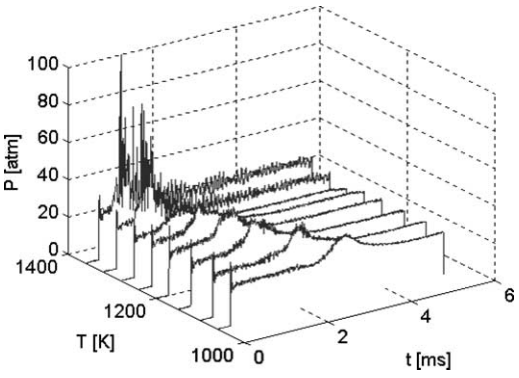

Fig. 2. Pressure history of ignition behind reflected shock ($P_5 = 23$ atm).

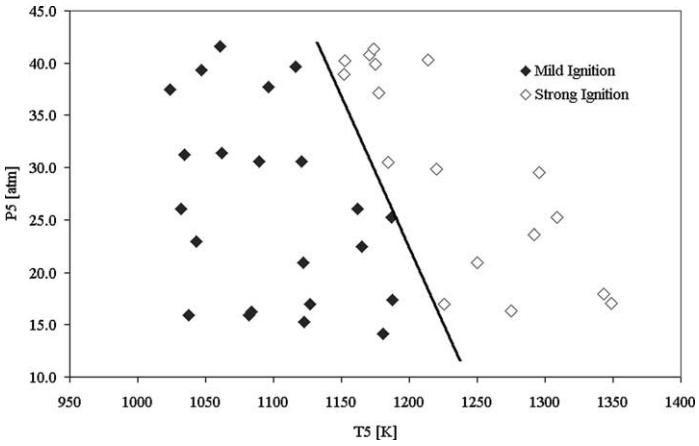

Fig. 3. Strong ignition limit of mixture No. 1 at different pressures. Filled symbols designate measured mild ignitions; open symbols designate measured strong ignition.

to the engine. In contrast, a strong ignition that forms the detonation-like pressure rise commonly termed "knock" [27] may cause severe damage to the engine.

Cheng and Oppenheim [7] attributed the cause of strong ignition to "coherence in the exothermic processes," which produces a sufficiently strong power per unit mass to generate a blast wave. They found that a "crucial factor" in establishing the strong ignition limit is the sensitivity of the induction time to temperature variation, i.e., the value of $(\partial\tau/\partial T)_p$. At a given pressure, when $(\partial\tau/\partial T)_p$ is small, which means the ignition delay is less sensitive to the standard deviation of the temperature field, "coherence" of ignition is more likely to occur, which will lead to a strong ignition.

Figure 3 shows the P-T conditions at which strong and mild ignitions were measured in mixture No. 1. For the stoichiometric mixture investigated, the values of $(\partial\tau/\partial T)_p$ derived from fitting the experimental data (which correspond to the measured strong ignition limit from 1220 to 1110 K with the initial pressure rising from 16 to 40 atm) changes from -4.0 to -6.0 μs/K. They are lower than the -1.5 to -2 μs/K reported by Cheng and Oppenheim based on their experiments conducted at 1 to 3 atm. It is readily understood that for a higher reactant concentration, the energy released by the ignition of per unit volume of gas mixture is higher. The requirement for the coherent exothermal process is lower. This allows a strong ignition to occur at a relatively lower $(\partial\tau/\partial T)_p$ value. For mixture No. 2 ($\Phi = 0.7$), the temperature limit measured is 1300 K at 16 atm and 1240 K at 40 atm, and the value of $(\partial\tau/\partial T)_p$ increases to -2.5 and -3.1 μs/K, respectively, which is a result of the reduced energy density in the lean mixtures.

3.2. Ignition delay

The ignition delay times obtained in the current experiments are summarized in Table 3. The measured ignition delay times at initial pressures from 16 to 40 atm in mixtures No. 1 and No. 2 are plotted in Figs. 4 and 5. The differences in ignition delay time measured at various pressures are more significant at lower temperatures than that at higher temperatures. Under the current conditions, the global activation energy, which is mainly a measurement of the temperature dependence of ignition delay time (there is also a weaker concentration dependence for a given pressure), shows a trend of reduction with decreasing temperature; however, for temperatures below 1100 K, a noticeable re-increase in the activation energy is observed. For temperatures between 1300 and 1200 K, the activation energy obtained by fitting the experimental data is 16 kcal/mol; it reduces to 13 kcal/mol for temperatures between 1200 and 1100 K, but it rises to 18 kcal/mol for temperatures below 1100 K. In general, E_a in the current study is significantly lower than the typical values (43–52 kcal/mol) reported in the literature [4–9] for high-temperature and low-pressure conditions. Such a reduction in activation energy in the intermediate-to-low temperature range was reported in several earlier studies. Cowell and Lefebvre's experiment [30] conducted at temperatures below 1000 K and pressures between 7 and 10 atm in a flow reactor yielded 25 kcal/mol. Walker et al. [9] reported that for stoichiometric methane/air mixtures at 960 to 1605 K and 1.5 to 15 atm, the global activation energy was 20 kcal/mol. Karim and Zhou [15] used a detailed mechanism to simulate the ignition process of methane and suggested using three different values (37, 21, 18 kcal/mol decreasing with temperature) for the activation energy in differ-

Table 3
Summary of experimental results

Φ	Mixture	T_5 (K)	P_5 (atm)	τ (μs)
1	1	1024	37.5	2712
1	1	1047	39.3	2217
1	1	1061	41.6	1212
1	1	1096	37.7	1080
1	1	1116	39.7	978
1	1	1152	38.9	714
1	1	1153	40.2	696
1	1	1171	40.8	660
1	1	1174	41.4	651
1	1	1175	39.9	612
1	1	1177	37.1	624
1	1	1213	40.3	612
1	1	1295	36.5	395
1	1	1035	31.2	2166
1	1	1062	31.4	1434
1	1	1090	30.5	1080
1	1	1121	30.6	1050
1	1	1184	30.5	888
1	1	1220	29.8	684
1	1	1296	29.6	414
1	1	1032	26.1	2343
1	1	1043	22.9	1698
1	1	1122	21.0	1560
1	1	1162	26.0	1164
1	1	1187	25.2	1149
1	1	1165	22.5	1000
1	1	1250	20.9	624
1	1	1309	25.2	489
1	1	1292	23.6	460
1	1	1038	15.9	3378
1	1	1084	16.2	1998
1	1	1082	16.0	2172
1	1	1122	15.3	1923
1	1	1127	17.0	1536
1	1	1181	14.1	1428
1	1	1188	17.4	1530
1	1	1226	17.0	1056
1	1	1275	16.4	600
1	1	1348	17.0	414
1	1	1343	17.9	444
0.7	2	1004	37.9	1728
0.7	2	1030	37.6	1668
0.7	2	1029	38.7	1548
0.7	2	1057	37.6	1416
0.7	2	1114	39.1	1050
0.7	2	1233	38.8	798
0.7	2	1288	39.1	694
0.7	2	1329	39.1	534
0.7	2	1370	38.8	456
0.7	2	1059	31.1	2154
0.7	2	1085	31.7	1422
0.7	2	1084	31.6	1392
0.7	2	1114	32.3	1362
0.7	2	1116	31.2	1464
0.7	2	1147	30.5	1176
0.7	2	1180	30.7	1092
0.7	2	1213	30.4	822
0.7	2	1286	31.0	714
0.7	2	1143	16.0	2022
0.7	2	1180	16.4	1482
0.7	2	1208	16.8	1158
0.7	2	1213	14.9	984
0.7	2	1304	15.7	690
1.3	3	1068	39.4	2028
1.3	3	1128	37.7	972
1.3	3	1193	39.2	930
1.3	3	1229	38.6	708
1.3	3	1266	36.0	612
1.3	3	1290	38.4	506

ent temperature ranges. Petersen et al. [31] reported that the activation energy for highly diluted CH_4–O_2 mixtures over a temperature range from 1175 to 1880 K was 47.0 kcal/mol; for lesser diluted mixtures [12,13], they found that the activation energy changed from 32.7 kcal/mol for temperatures over 1300 K to 19 kcal/mol for temperatures below. The reversed-'S'-shape characteristic observed in the current study and a negative temperature-dependent region are also shown in the results of Petersen et al. [12,13] for rich methane/oxygen/argon mixtures. The current results seem to agree with the low values of the activation energy reported in above studies.

Figures 6 and 7 plot the effects of equivalence ratio on the ignition delay time at different pressures. At 16 atm, the increase of activation energy in the lean mixture occurs at a higher temperature than in the stoichiometric mixture; however, the situation reverses when the initial pressure is increased to 40 atm, where the ignition delay of mixture No. 2 appears to be least sensitive to the temperature change—no significant variation in the activation energy is found in the temperature range investigated. At low temperatures ($T < 1050$ K), the lean mixture shows a considerably shorter ignition delay time than do stoichiometric and rich mixtures. For temperatures above 1200 K, ignition occurs slower in the lean mixture than in the rich and stoichiometric mixtures.

Given the varying activation energy at different temperatures and pressures in the current study, we found it difficult to correlate measured ignition delay times with initial conditions using any one-step, parametric equation. Analyses of detailed chemical kinetic models are necessary to obtain a better understanding of methane oxidation under current the conditions.

3.3. Kinetic modeling

Most of the existing detailed reaction mechanisms [14,32–35] for methane oxidation were optimized

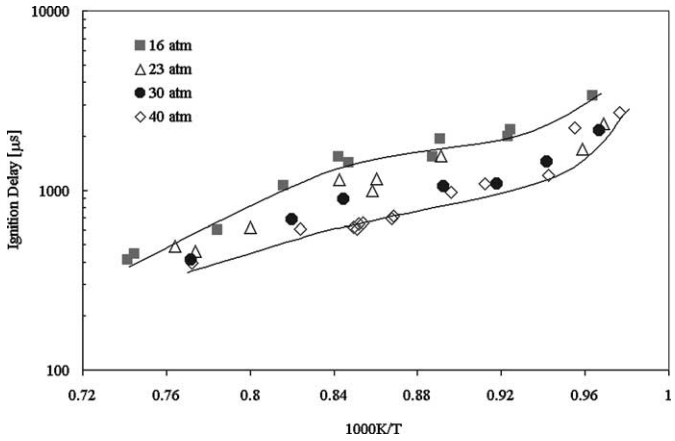

Fig. 4. Measured ignition delay time in mixture No. 1 (stoichiometric) at different initial pressures.

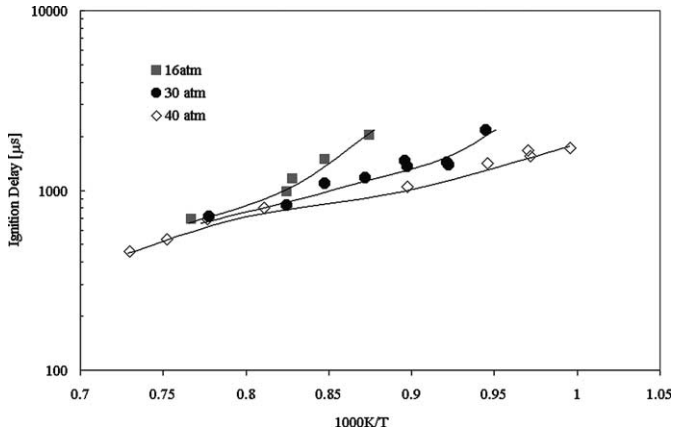

Fig. 5. Measured ignition delay time in mixture No. 2 (lean) at different initial pressures.

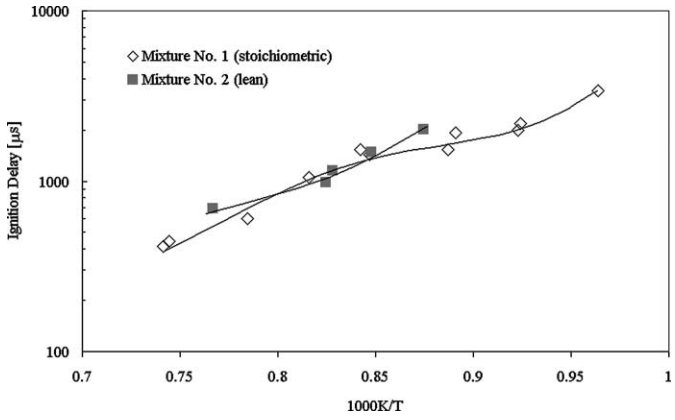

Fig. 6. Comparison of ignition delay for mixtures No. 1 and 2 at 16 atm.

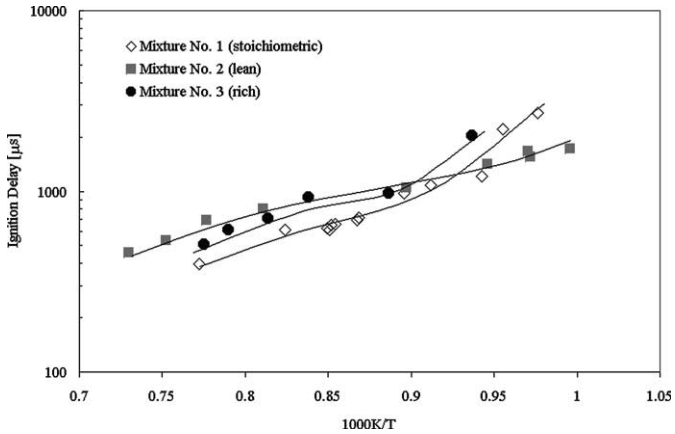

Fig. 7. Comparison of ignition delay for mixtures No. 1, 2, and 3 at 40 atm.

and validated for high-temperature and low-pressure autoignition; few were developed for applications under conditions pertinent to the current study. High-pressure mechanisms for methane ignition were recently reported by Li and Williams [36] and Petersen et al. [13]. The Li and Williams [36] mechanism contains 30 species and 127 reactions (24- and 9-step reduced mechanisms are also presented). The reduction in activation energy at temperatures below 1300 K is attributed to the decreased significance of methane decomposition step—$CH_4(+M) \Leftrightarrow CH_3 + H(+M)$—at intermediate temperatures. The mechanism does not show a re-increase in activation energy at lower temperatures as observed in the current study. The kinetic mechanism developed by Petersen et al. [13] contains 38 species and 190 reaction steps with its core mechanism taken from GRI-Mech 1.2 [37]. Species that are important in low-temperature methane oxidation, including CH_3O_2, CH_3O_2H, C_2H_5O, $C_2H_5O_2$, $C_2H_5O_2H$, and CH_3CO, were added to the mechanism. It should be noted that the addition of some of these species, especially CH_3O_2, is also presented in some recently published mechanisms [38–40] for high-pressure, low-temperature oxidation of higher hydrocarbons. The Petersen et al. [13] mechanism was validated with the ignition delay data [11,12] for $CH_4/O_2/Ar$ and $CH_4/O_2/N_2$ mixtures at high pressures (40–260 atm) and intermediate temperatures (1040–1500 K). The experiments below 1200 K were mostly focused on fuel-rich conditions with equivalence ratios ranging from 3 or 6. The model presents a significantly improved agreement with the experimental data of the present study compared to the core mechanism (GRI-Mech 1.2). However, a relatively large deviation from the experimental results is observed at the lowest temperatures (< 1100 K); a similar increase in the disagreement is also seen in results of Li and Williams [36]. No analytical or experimental results were presented for stoichiometric methane/air mixtures under engine-relevant conditions using either of these mechanisms. In the current study, the Petersen et al. mechanism [13] was taken as the base mechanism for kinetic modeling.

To improve the performance of the mechanism, important elementary reactions were identified by comparing kinetic and thermal contributions of elementary reactions throughout the induction period at various initial conditions. This technique is commonly used in mechanism reduction [41–43]. Selected values of rate coefficients obtained from the literature were tested for key reactions to improve the agreement between the model and the experimental results, particularly at the lowest temperatures (< 1100 K). As a result, the following modifications to the original mechanism were implemented:

1. Reaction 157 was replaced by its reverse reaction—$HO_2 + CH_4 \Leftrightarrow CH_3 + H_2O_2$—whose reaction rate coefficients were taken from the methane-oxidation mechanism suggested by Hunter et al. [44]. Their mechanism was optimized to match the species profile in a flow reactor at moderate temperatures (930 to 1000 K) and elevated pressures (6 to 10 atm).

2. The rate coefficients of reaction 179 were modified using values from Tsang and Hampson [45], but the rate constant was reduced by a factor of 4 to match the current experimental results better. As was pointed out by Petersen et al. [13], there remains a large uncertainty in rate of this reaction. No direct measurement of the reaction rate in the current temperature range was found in our review. The above adjustment of the rate coefficient is well within the uncertainty of the data reported in the literature [45–47].

3. Two extra reactions involving CH_3O_2 were added:

$$CH_3O_2 + HO_2 \Leftrightarrow CH_3O_2H + O_2 \quad \text{(R191)}$$

and

Table 4
Modified or extended reactions and reaction rate coefficients (based on Petersen et al. [13] mechanism)

No.	Reaction	A	n	E (cal/mol)	Ref.
R157	$HO_2 + CH_4 \Leftrightarrow CH_3 + H_2O_2$	4.48E + 13	0.0	24629.0	[44]
R179	$CH_3 + O_2 \Leftrightarrow CH_3O_2$	2.13E + 58	−15.0	17018.0	[45]
R191	$CH_3O_2 + HO_2 \Leftrightarrow CH_3O_2H + O_2$	4.60E + 10	0.0	2600.0	[40]
R192	$CH_3O_2 + CH_3O_2 \Leftrightarrow O_2 + 2CH_3O$	3.70E + 11	0.0	2200.0	[40]

Table 5
Comparison of thermochemical properties of CH_3O_2 from different sources

Source of database	$\Delta H_{f,298}$ (kcal/mol)	$C_{p,298}$ (cal/(mol K))	$C_{p,1000}$ (cal/(mol K))	S_{298} (cal/(mol K))
Petersen et al. [13]	5.66	17.55	24.55	60.35
Burcat [42]	2.14	12.76	24.18	64.39
Curran [46]	4.295	13.88	22.60	66.28

$$CH_3O_2 + CH_3O_2 \Leftrightarrow O_2 + CH_3O + CH_3O \quad \text{(R192)}$$

were taken from the DME mechanism developed by Curran et al. [38]. The mechanism has been validated with species-profile as well as ignition-delay data measured at high pressure (10–40 atm) and low to moderate temperatures (800–1300 K). The reaction-rate analysis shows the relative importance of these two reactions under the current experimental conditions. A summary of elementary reactions modified/added in the current study is given Table 4.

The thermochemical properties for the species not included in GRI-Mech (CH_3O_2, CH_3O_2H, C_2H_5O, $C_2H_5O_2$, $C_2H_5O_2H$, and CH_3CO) were taken either from the latest database of Burcat [48] or from that provided by Curran et al. [38]. It should be noted that some data used in the current modeling are significantly different from those used by Petersen et al. [13]. Comparisons of the standard enthalpy of formation and constant-pressure specific heat for CH_3O_2 from different sources are presented in Table 5. It can be seen that at 1000 K, values of enthalpy and Cp for CH_3O_2 used by Petersen et al. [13] are significantly higher than those reported by Burcat [48] and Curran et al. [38]. This leads to a higher calculated reverse rate of R179 as a result of a smaller equilibrium constant [49] and, consequently, a lower formation rate of CH_3O_2. It is thus important to clarify that the "base mechanism" (that is, the original mechanism prior to the modification just described) in the following discussion is not the same as the "Petersen et al. [13] mechanism" due to the difference in the thermochemistry—the resulting ignition delay times can be varied by a factor of 2 using different thermodynamic data under the same conditions.

The current calculation was performed using ideal-gas Chemkin [50]. Petersen et al. [13] showed that the difference between using the ideal-gas state equation and real-gas state equation was below 4 to 5% even for initial pressures above 200 atm. The constant-volume, adiabatic boundary conditions, which were adopted by several previous researchers [4,14,26], were used in the current calculation. The stiff ODE system composed of species mass conservation and energy conservation equations was solved using VODE—a variable-coefficient ODE solver developed by Brown et al. [51]. The ignition was defined using the same pressure criterion as aforementioned in the experiment.

3.4. Numerical results

Comparisons between the predicted ignition delay time from the current model and the experimental measurements are presented in Figs. 8 to 12. The agreement between the model and the experiment is generally good. For stoichiometric methane/air mixtures, the model correctly reproduces the reduction in activation energy with decreasing temperature up to 1150 K. For temperatures below 1100 K, the model predicts the re-increase in the activation energy, which was observed in the experiment. As a comparison, the ignition delay times predicted by the base mechanism and the latest version of the GRI mechanism—GRI-Mech 3.0—are also presented. The current model shows a significant improvement in performance relative to the base mechanism. The results from the GRI mechanism, which was not designed for low-temperature reactions, appear to deviate significantly from the experimental data with decreasing temperature. The mechanism fails to predict the change in the activation energy under the current conditions.

In Figs. 11 and 12, the model is compared to the experiment for the ignition delay in the lean mixture (mixture No. 2). The change in activation energy for the lean mixture is less prominent than that for the

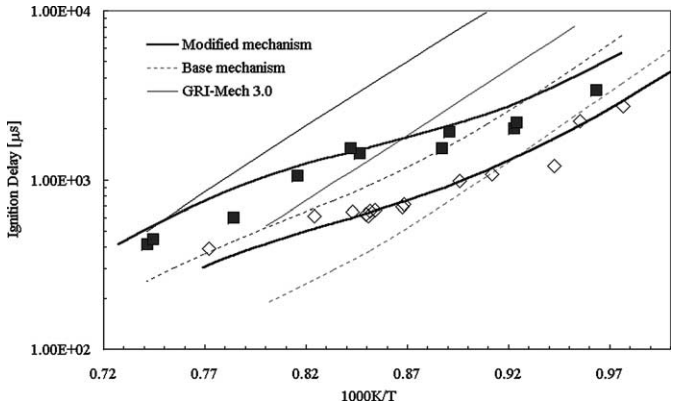

Fig. 8. Comparison of model-predicted and experimental ignition delay in mixture No. 1 (stoichiometric) at 16 and 40 atm. Symbols are experimental data from the current study: squares, data at 16 atm; diamonds, data at 40 atm.

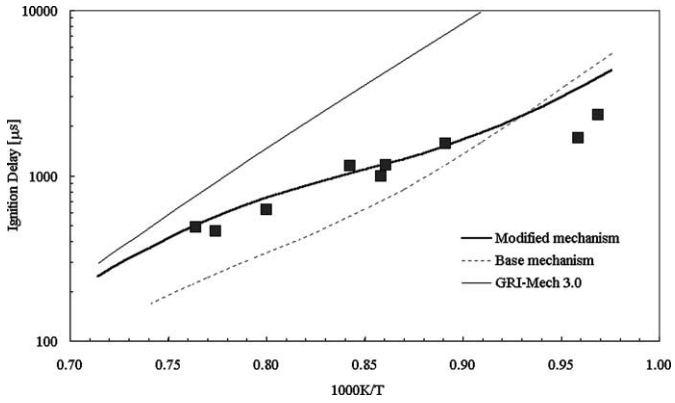

Fig. 9. Comparison of model-predicted and experimental ignition delay in mixture No. 1 (stoichiometric) at 23 atm. Symbols are experimental data from the current study.

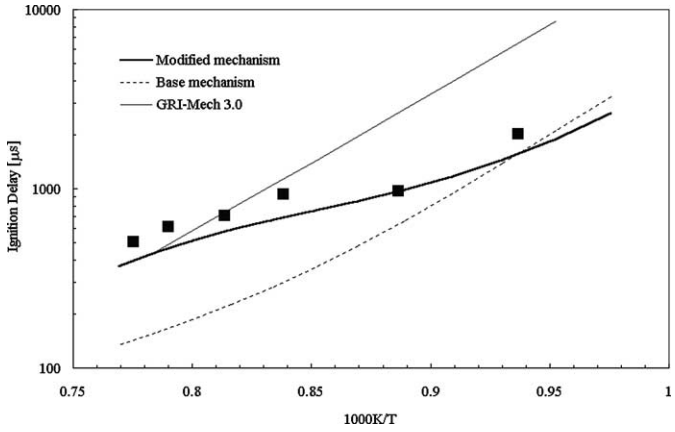

Fig. 10. Comparison of model-predicted and experimental ignition delay in mixture No. 3 (rich) at 40 atm. Symbols are experimental data from the current study.

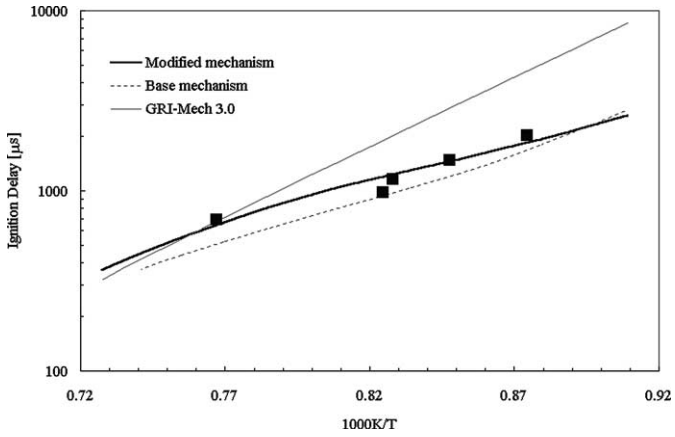

Fig. 11. Comparison of model-predicted and experimental ignition delay in mixture No. 2 (lean) at 16 atm. Symbols are experimental data from the current study.

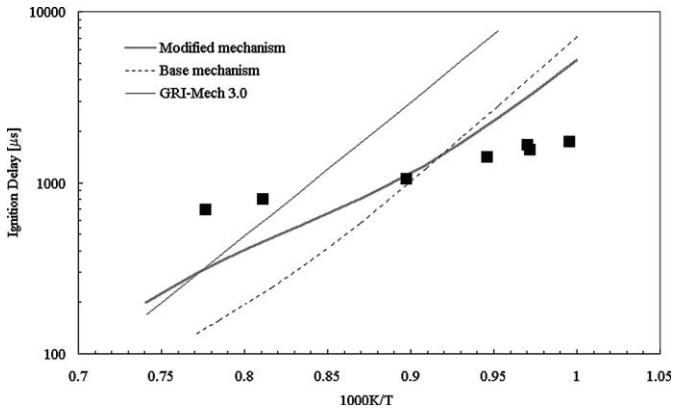

Fig. 12. Comparison of model-predicted and experimental ignition delay in mixture No. 2 (lean) at 40 atm. Symbols are experimental data from the current study.

stoichiometric mixtures. The agreement between the model and experiment is good at 16 atm; however, the model over-predicts the activation energy at 40 atm, while the experimental data show that the ignition is less sensitive to temperature at high pressures.

For rich methane/air and methane/oxygen/argon mixtures, the model was compared with the current results as well as the measurement reported by Petersen et al. [12] (Figs. 13 and 14). A satisfactory agreement is also achieved, although the model appears to under-predict the ignition delay time of mixture No. 3 slightly. The maximum deviation of the model results from the experimental data is less than 20%.

Figure 15 presents the ignition delay time predicted by the current model under high-temperature and low-pressure conditions. They are compared with the experimental results reported by Seery and Bowman [4]. It can be seen that the current modification does not significantly affect the precision of the original mechanism in the region where it has been optimized and extensively validated.

3.5. Reaction flow and sensitivity analysis

Integral reaction flow analyses [49] were conducted to identify the main reaction path for the oxidation of methane in mixture No. 1 during the induction period for initial temperatures of 1050 and 1250 K respectively. The integration was carried out to approximately 11% fuel conversion. Hunter et al. [52] used this criterion and found that it represented the pre-ignition reactions well. As presented in Fig. 16, the most important intermediate species and the sequence of oxidation for the stoichiometric mixture are very similar to those of rich mixtures shown by Petersen et al. [13]. During the induction period at 1250 K, a majority of methane is converted to methyl though the attack of OH radicals. A smaller fraction of methane is consumed in reactions with

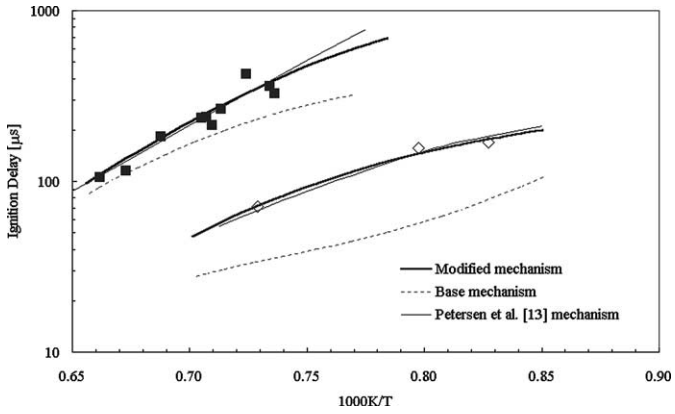

Fig. 13. Comparison of model-predicted and experimental ignition delay for a $0.20CH_4/0.133O_2/0.667Ar$ mixture at 40 and 170 atm. Symbols are experimental data from Petersen et al. [12].

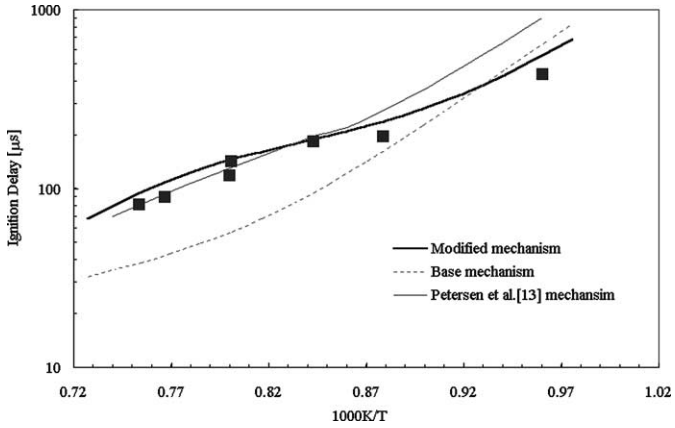

Fig. 14. Comparison of model-predicted and experimental ignition delay for a $0.273CH_4/0.182O_2/0.545N_2$ mixture at 130 atm. Symbols are experimental data from Petersen et al. [12].

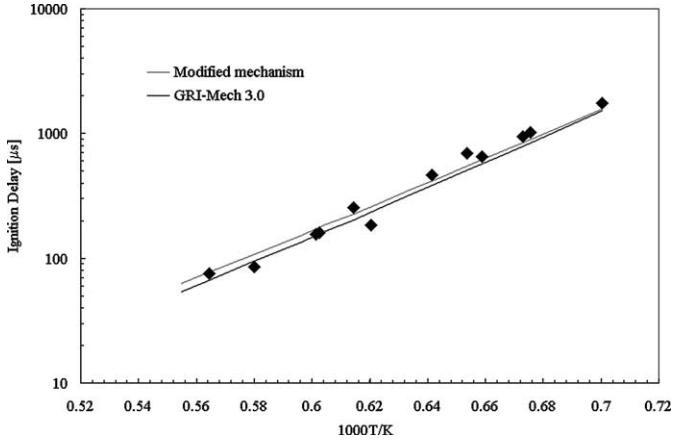

Fig. 15. Comparison of model-predicted and experimental ignition delay under low-pressure and high-temperature conditions. Symbols are experimental data from Seery and Bowman [4].

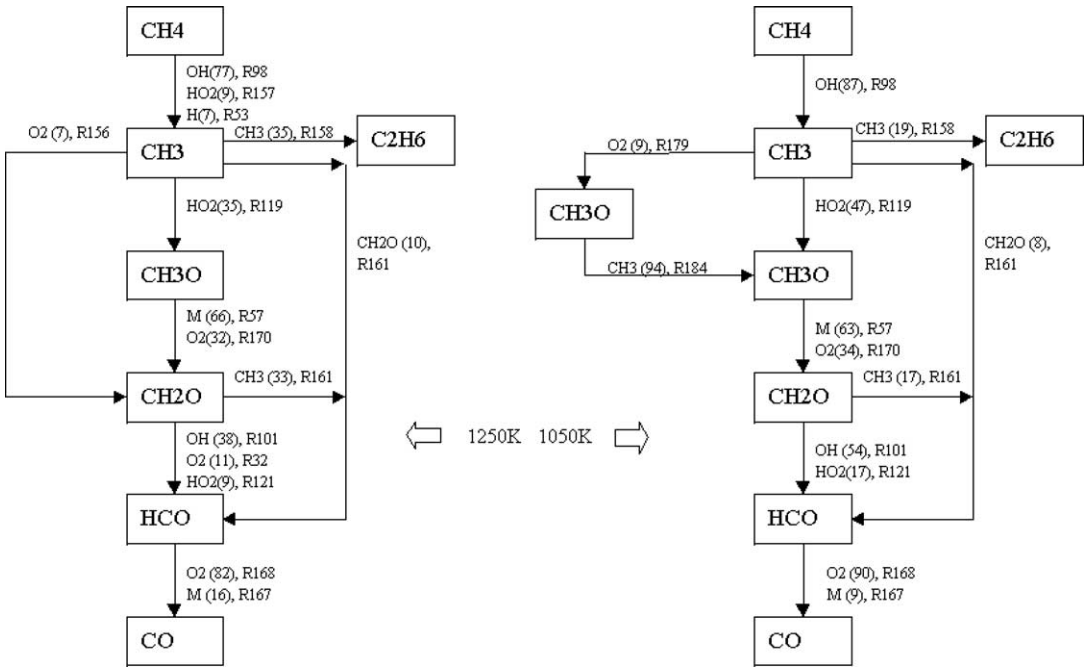

Fig. 16. Main reaction pathways for methane oxidation in mixture No. 1 at 1250 and 1050 K (40 atm). Numbers in parentheses are mole percentages of species consumed in specified reactions.

HO_2, H, and O radicals. But the subsequent oxidation of methyl to form methoxy, CH_3O, is mainly through reacting with HO_2 radicals in

$$HO_2 + CH_3 \Leftrightarrow OH + CH_3O \quad (R119).$$

This is followed by a rapid oxidation of methoxy in

$$H + CH_2O(+M) \Leftrightarrow CH_3O(+M) \quad (R57)$$

and

$$CH_3O + O_2 \Leftrightarrow HO_2 + CH_2O \quad (R170).$$

The above two reactions have larger rates than R119. This is evident in the species concentration history shown in Fig. 17. The concentration of formaldehyde during the induction period is higher than that of methoxy by nearly 4 orders of magnitude. A quasi-steady state approximation applies to such a situation [49], in which the overall reaction rate is determined by the rate of R119.

A parallel path with the above reactions for the formation of formaldehyde is through

$$CH_3 + O_2 \Leftrightarrow OH + CH_2O \quad (R156).$$

It can be seen from Fig. 18 that the rate of R156 increases rapidly during the initial stage of the induction period, but it slows down relative to R119 with the shift of equilibrium due to the increasing CH_2O concentration. Another main reaction that consumes methyl radicals is

$$CH_3 + CH_3 \Leftrightarrow C_2H_6 \quad (R158),$$

which is a well-known chain-termination reaction discussed in many previous works [14,53–55]. At 1250 K, nearly 36% of methyl radicals are consumed in R158, making it a main ignition-inhibiting step. The lower branch of C_2 oxidation is less significant in low-temperature methane-oxidation reactions and is usually not included in reduced mechanisms [36,55].

The lower part of the oxidation path, as shown by Frenklach and Bornside [26], is an autocatalytic process. The oxidation of CH_2O proceeds through reactions with OH in

$$OH + CH_2O \Leftrightarrow HCO + H_2O \quad (R101)$$

and with CH_3 in

$$CH_3 + CH_2O \Leftrightarrow HCO + CH_4 \quad (R161).$$

This is followed by the oxidation of HCO via R167 and R168:

$$HCO + M \Leftrightarrow H + CO + M \quad (R167),$$

$$HCO + O_2 \Leftrightarrow HO_2 + CO \quad (R168).$$

Reactions R167 and R168 restore the concentration of active radicals, i.e., H, HO_2; these two reactions are also highly exothermic, which makes them efficient in promoting ignition.

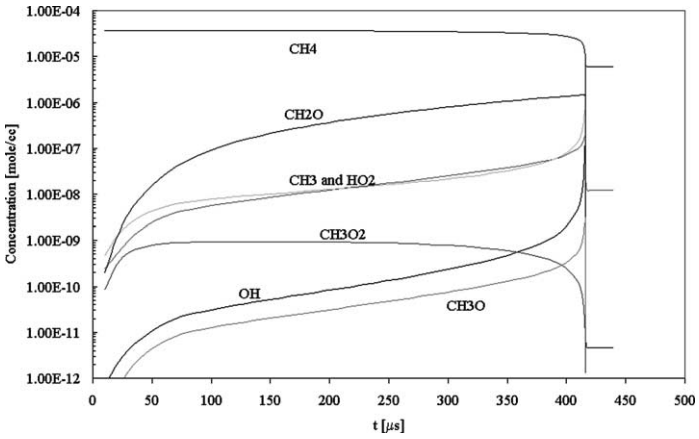

Fig. 17. Species concentration history for mixture No. 1 at 1250 K and 40 atm.

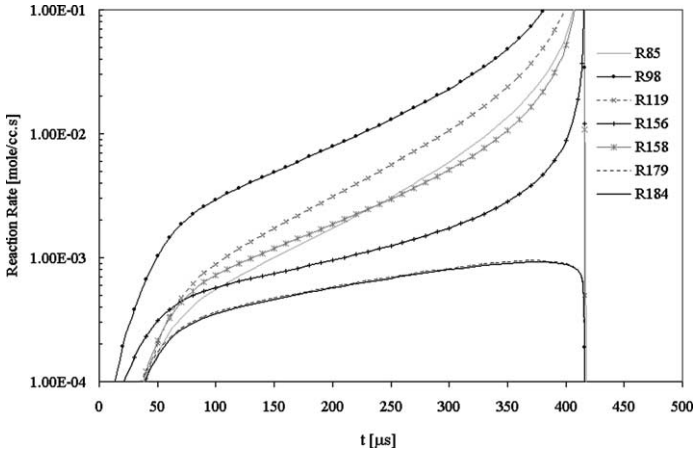

Fig. 18. Reaction rates during the induction period of mixture No. 1 at 1250 K and 40 atm.

Two of the most important active radicals for methane oxidation are OH and HO_2. OH is formed mainly through

$$H_2O_2(+M) \Leftrightarrow 2OH(+M) \quad \text{(R85)}$$

and R119, while HO_2 radicals are mostly generated in R168, R170 and

$$H + O_2 + N_2 \Leftrightarrow HO_2 + N_2 \quad \text{(R36)}.$$

Because R119 is important in both consuming methyl and generating hydroxyl radicals, its relatively slow rate makes it a main rate-limiting reaction for methane ignition at 1250 K.

The most prominent difference between lower-temperature and higher-temperature methane oxidation is the increasing significance of CH_3O_2 as a chain carrier. A parallel pathway to R119 in generating CH_3O from CH_3 is through

$$CH_3 + O_2 \Leftrightarrow CH_3O_2 \quad \text{(R179)}$$

and

$$CH_3O_2 + CH_3 \Leftrightarrow 2CH_3O \quad \text{(R184)}.$$

At 1050 K, although most of the methyl radicals are still consumed via R119, the reaction-rate plot in Fig. 19 shows that R184 actually dominates the first half of the induction period in converting methyl to methoxy. The fraction of methyl destroyed through recombination in R158 is significantly reduced as a result of the competition from R179 and R184. The increasing significance of CH_3O_2 chemistry at lower temperatures is attributed to the rapid rise of the rate of R179, which is accompanied by the reduction in the global activation energy as presented in Fig. 20. For a temperature increase from 1050 to 1250 K, the rate of reaction R179 increases by nearly a factor of 5.

Figure 21 shows the sensitivity of the ignition delay time to the change of forward rate constants of elementary reactions. It is interesting to notice that although the rate of reaction R179 is high at low tem-

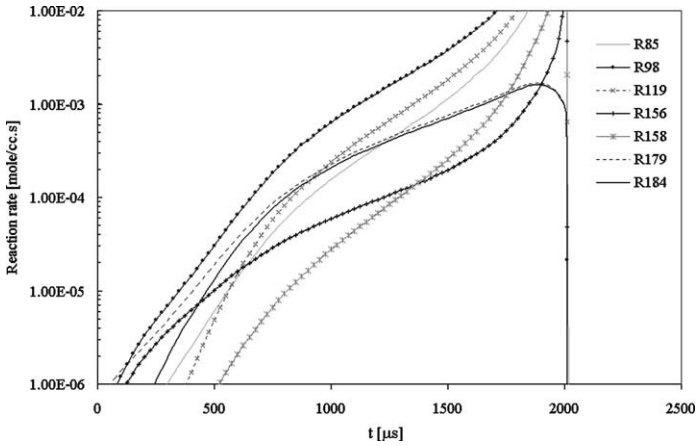

Fig. 19. Reaction rates during the induction period of mixture No. 1 at 1050 K and 40 atm.

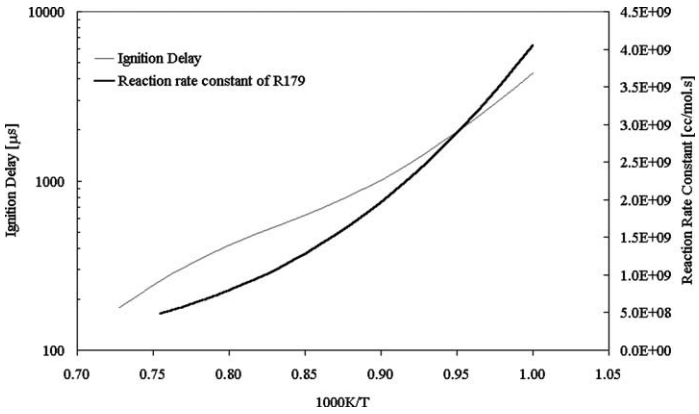

Fig. 20. Change in reaction rate constants of R179 with temperature and corresponding ignition delay time at 40 atm.

peratures, the ignition delay time is more sensitive to the change in k_{179} at 1250 K than it is at 1050 K. For the latter, the ignition delay is more sensitive to R157 and R85. Also, the sensitivity to the rate of R98, a main methyl-generating reaction, changes its sign from rate-limiting to rate-promoting with the reduction of temperature. The reduced promotion efficiency of CH_3O_2 radicals at low temperatures suggests a shift of the rate-limiting reactions from those consuming methyl radicals (e.g., R119) to those generating methyl and hydroxyl radicals (R98, R85) with the rise of R179 and R184; in other words, with a higher rate of R179 at lower temperatures, the overall reaction rate is increasingly limited by the depletion of methyl and hydroxyl radicals. This is evident in a comparison of methyl and hydroxyl concentrations at 1050 K with those at 1250 K (see Fig. 22). The reduced concentration of hydroxyl at 1050 K is mainly a consequence of the competition between R119 and R179 for methyl radicals. This leads to the reduction in the rate of R98 and slows down the chain initiation step. The shift of the rate-limiting steps accounts for the re-increase of the activation energy at the lowest temperatures in both experimental and numerical results.

It should be noted that R184 favors fuel-rich and stoichiometric mixtures where the concentration of CH_3 is higher than that in lean mixtures. This is clear from the calculated ignition delay times of lean mixtures, which are significantly longer than those of richer mixtures. Although the current model demonstrates an improved agreement between numerical and experimental results, the fact that the model does not predict accurately the ignition delay time of lean mixtures at the highest pressures indicates the necessity for further kinetic studies. Large uncertainties remain in some important elementary reactions. R179, for example, is a bimolecular reaction in its current form; however, third body effects were considered in kinetic models of some recent studies [38–40]; the enhancement coefficients for different species including oxygen for this reaction have not been thoroughly studied.

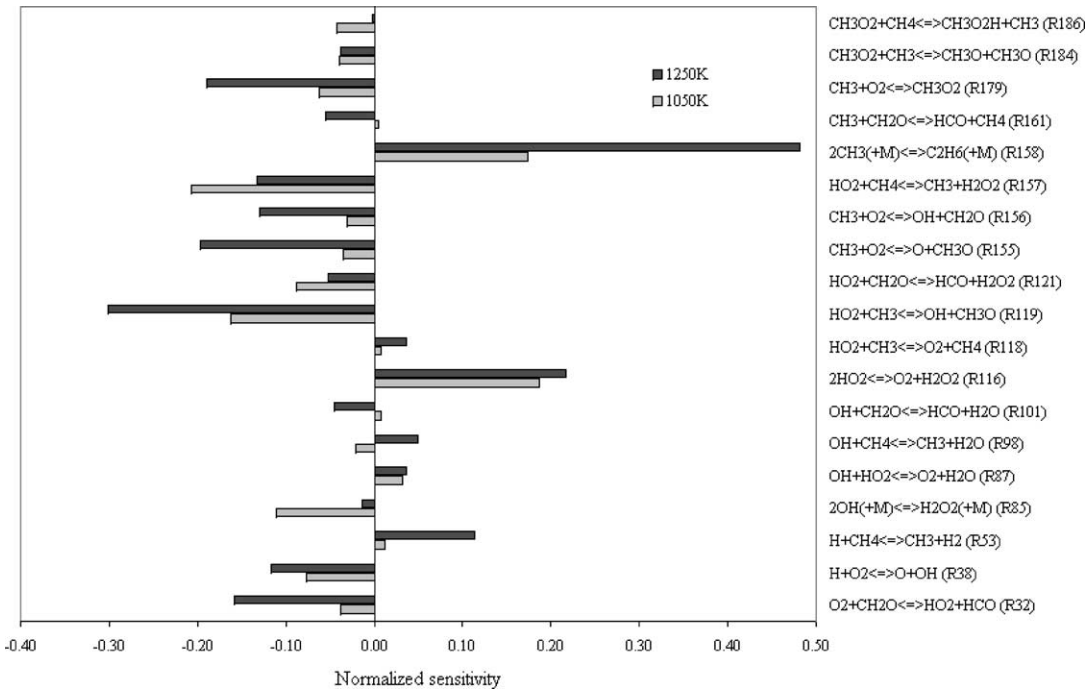

Fig. 21. Brute force sensitivity for ignition delay time at 40 atm ($k \times 2$).

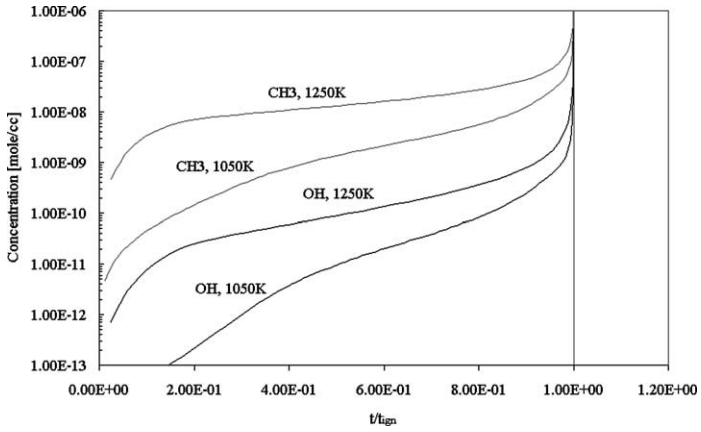

Fig. 22. Comparison of hydroxyl and methyl concentrations at 1050 and 1250 K during the induction period.

4. Summary and conclusions

Shock-tube experiments on CH_4/air ignition were conducted under engine-relevant conditions. The strong ignition limit was measured. High reactant concentrations are found to favor strong ignitions and cause an increase in the critical value of $(\partial\tau/\partial T)_p$ at the strong ignition limit. A nonlinear behavior of measured ignition delay time in the Arrhenius representation under the current conditions is observed. The global activation energy decreases with decreasing initial temperature up to 1150 K, but increases at temperatures below 1100 K. The nonlinearity is more pronounced in stoichiometric mixtures than it is in lean mixtures.

A detailed chemical kinetic model based on the Petersen et al. [13] mechanism containing 38 species and 192 reactions was used to study pre-ignition reactions. A good agreement is achieved between model-predicted and experimental ignition delay for stoichiometric and rich mixtures. The model correctly reproduces the reversed-'S'-shape characteristic of the ignition delay data. However, relatively large deviations are found when the model is used to pre-

dict the ignition delay time of lean mixtures at the highest pressures. Sensitivity and integral reaction flow analyses were carried out to study the oxidation path of methane. For stoichiometric methane/air mixtures at 40 atm and 1250 K, the oxidation is mainly rate-limited by reactions consuming methyl radicals. At lower temperatures, the rate of $CH_3 + O_2 \Leftrightarrow CH_3O_2$ increases rapidly; this reaction, together with $CH_3O_2 + CH_3 \Leftrightarrow 2CH_3O$, opens an effective, parallel channel in converting methyl to methoxy, which significantly promotes the ignition and leads to the reduction in the activation energy. At still lower temperatures, the depletion of methyl and hydroxyl radicals becomes increasingly rate-limiting and causes the activation energy to re-increase even though the formation rate of CH_3O_2 radicals is high.

Acknowledgments

This work was jointly funded by the National Science and Engineering Research Council of Canada (NSERC) and Westport Innovations Inc. of Vancouver, Canada.

References

[1] A. Gangopadhyay, P. Meckl, J. Dyn. Syst.—Trans. ASME 123 (2001) 425–430.
[2] A. Ishida, A. Nishimura, M. Uranishi, R. Kihara, A. Nakamura, P. Newman, JSAE Rev. 22 (2001) 237–243.
[3] P. Ouellette, High-pressure direct injection of natural gas in diesel engines, in: Proceedings of NGV 2000, NGV—Transportation for the New Century, Seventh International Conference and Exhibition on Natural Gas Vehicles, International Association For Natural Gas Vehicles, Inc., Yokohama, Japan, 2000, pp. 235–241.
[4] D.J. Seery, C.T. Bowman, Combust. Flame 14 (1970) 37–47.
[5] A. Lifshitz, K. Scheller, A. Burcat, G.B. Skinner, Combust. Flame 16 (1971) 311–321.
[6] T. Tsuboi, H.G. Wagner, Proc. Combust. Inst. 15 (1974) 883.
[7] R.K. Cheng, A.K. Oppenheim, Combust. Flame 58 (1984) 125–139.
[8] A. Grillo, M.W. Slack, Combust. Flame 27 (1976) 377–381.
[9] D.W. Walker, L.H. Diehl, W.A. Strauss, R. Edse, Investigation of ignition properties of flowing combustible gas mixtures, Report No. AFAPL-TR-69-82, USAF Report, 1969.
[10] N. Lamoureux, C.E. Paillard, V. Vaslier, Shock Waves 11 (2002) 309–322.
[11] E.L. Petersen, M. Röhrig, D.F. Davidson, R.K. Hanson, C.T. Bowman, Proc. Combust. Inst. 26 (1996) 790–806.
[12] E.L. Petersen, D.F. Davidson, R.K. Hanson, J. Prop. Power 15 (1) (1999) 82–91.
[13] E.L. Petersen, D.F. Davidson, R.K. Hanson, Combust. Flame 117 (1999) 272–290.
[14] A.G. Gaydon, I.R. Hurle, The Shock Tube in High Temperature Chemical Physics, Chapman and Hall, London, 1963, pp. 4–6, 30–32, 63–66.
[15] G.A. Karim, G. Zhou, J. Energy Res. Technol. 114 (1994) 175–189.
[16] G.P. Smith, D.M. Golden, M. Frenklach, N.W. Moriarty, B. Eiteneer, M. Goldenberg, C.T. Bowman, R.K. Hanson, S.S. Song, W.C. Gardiner, V.V. Lissianski, Z. Qin, GRI-MECH 3.0, http://www.me.berkeley.edu/gri_mech/.
[17] E.K. Dabora, Combust. Flame 24 (1975) 181–184.
[18] V.M. Zamansky, A.A. Borisov, Energy Combust. Sci. 18 (1992) 235–297.
[19] B.J. McBride, S. Gordon, M.A. Reno, Coefficients for calculating thermodynamic and transport properties of individual species, Report No. TM-4513, NASA, 1993.
[20] A. Burcat, B. McBride, 1994 ideal gas thermodynamic data for combustion and air-pollution use, Report No. TAE 697, Technion, 1993.
[21] G. Ben-Dor, O. Igra, T. Elperin, Handbook of Shock Waves, Vol. 1, Academic Press, New York, 2001, pp. 204, 573–580.
[22] J. Delery, J.G. Marvin, Shock-Wave Boundary Layer Interactions, Neuilly-sur-Seine, Agard, 1986, pp. 51–85.
[23] H. Mark, The interaction of a reflected shock wave with the boundary layer in a shock tube, Report No. TM 1418, NSCA, 1958.
[24] L. Davies, The interaction of the reflected shock with the boundary layer in a shock tube and its influence on the duration of hot flow in the reflected-shock tunnel, ARC paper, No. 880-881, 1967.
[25] G.B. Skinner, J. Chem. Phys. 31 (1959) 268.
[26] M. Frenklach, D.E. Bornside, Combust. Flame 56 (1984) 1–27.
[27] K. Fieweger, R. Blumenthal, G. Adomeit, Combust. Flame 109 (1997) 599–619.
[28] H.K. Ciezki, G. Adomeit, Combust. Flame 93 (1993) 431–443.
[29] K. Fieweger, R. Blumenthal, G. Adomeit, Proc. Combust. Inst. 25 (1994) 1579–1585.
[30] L.H. Cowell, A.H. Lefebvre, Influence of pressure on autoignition characteristics of gaseous hydrocarbon-air mixtures, SAE paper 860068, 1987.
[31] E.L. Petersen, D.F. Davidson, M. Rohrig, R.K. Hanson, Shock induced ignition of high-pressure H_2–O_2–Ar and CH_4–O_2–Ar mixtures, AIAA paper No. 95-3113, 1995.
[32] E. Lutz, A numerical study of thermal ignition, Report No. SAND88-8228, Sandia National Laboratories, 1988.
[33] A.E. Lutz, R.J. Kee, J.A. Miller, H.A. Dwyer, A.K. Oppenheim, Proc. Combust. Inst. 22 (1998) 1683–1693.
[34] P. Dagaut, J.C. Boettner, M. Cathonnet, Combust. Sci. Technol. 77 (1991) 127–148.
[35] Y. Hidaka, K. Sato, Y. Henmi, H. Tanaka, K. Inami, Combust. Flame 118 (1999) 340–358.

[36] S.C. Li, F.A. Williams, J. Eng. Gas Turbines Power—Trans. ASME 124 (3) (2002) 471–480.
[37] M. Frenklach, H. Wang, C.L. Yu, M. Goldenberg, C.T. Bowman, R.K. Hanson, D.F. Davidson, E.J. Chang, G.P. Smith, D.M. Golden, W.C. Gardiner, V. Lissianski, http://www.me.berkeley.edu/gri_mech/; Gas Research Institute Topical Report: M. Frenklach, H. Wang, M. Goldenberg, G.P. Smith, D.M. Golden, C.T. Bowman, R.K. Hanson, W.C. Gardiner, V. Lissianski, GRI-Mech—an optimized detailed chemical reaction mechanism for methane combustion, Report No. GRI-95/0058, November 1, 1995.
[38] H.J. Curran, W.J. Pitz, N.M. Marinov, C.K. Westbrook, P. Dagaut, J.-C. Boettner, M. Cathonnet, J. Chem. Kinet. 30 (1998) 229–241.
[39] S.Q. Wang, D.L. Miller, N.P. Cernansky, H.J. Curran, W.J. Pitz, C.K. Westbrook, Combust. Flame 118 (1999) 415–430.
[40] H.J. Curran, P. Gaffuri, W.J. Pitz, C.K. Westbrook, Combust. Flame 114 (1998) 149–177.
[41] H. Wang, M. Frenklach, Combust. Flame 87 (1991) 365–370.
[42] M. Frenklach, K. Kailasanath, E.S. Oran, Progr. Astronautics Aeronautics 105 (2) (1986) 365–376.
[43] M. Frenklach, Progr. Astronautics Aeronautics 135 (1991) 129–154.
[44] T.B. Hunter, H. Wang, T.A. Litzinger, M. Frenklach, Combust. Flame 97 (1994) 201–224.
[45] W. Tsang, R.F. Hampson, J. Phys. Chem. Ref. Data 15 (1986) 1087.
[46] D.L. Baulch, C.J. Cobos, R.A. Cox, C. Esser, P. Frank, Th. Just, J.A. Kerr, M.J. Pilling, J. Troe, R.W. Walker, J. Warnatz, J. Phys. Chem. Ref. Data 21 (1992) 411–429.
[47] A.M. Dean, P.R. Westmoreland, Int. J. Chem. Kinet. 19 (1987) 207.
[48] A. Burcat, Third millennium ideal gas and condensed phase thermochemical database for combustion, Technion Aerospace Engineering (TAE) Report 867, January 2001; also see Alexander Burcat's Ideal Gas Thermochemical Database, ftp://ftp.technion.ac.il/pub/supported/aetdd/thermodynamics; date mirrored at http://garfield.elte.chem/Burcat/burcat.html.
[49] J. Warnatz, U. Maas, R.W. Dibble, Combustion, second ed., Springer-Verlag, New York, 1999, pp. 67, 95–97.
[50] R.J. Kee, F.M. Rupley, J.A. Miller, Chemkin-II: a Fortran chemical kinetics package for the analysis of gas-phase chemical kinetics, Report No. SAND89-8009, UC-401, Sandia National Laboratories, 1989.
[51] P.N. Brown, G.D. Byrne, A.C. Hindmarsh, SIAM J. Sci. Stat. Comput. 10 (1989) 1038–1051; also, LLNL Report UCRL-98412, June 1988.
[52] T.B. Hunter, T.A. Litzinger, H. Wang, M. Frenklach, Combust. Flame 104 (1996) 505–523.
[53] D.F. Cooke, A. Wiliams, Proc. Combust. Inst. 13 (1970) 757–765.
[54] L.J. Spadaccini, M.B. Colket III, Prog. Energy Combust. Sci. 20 (1994) 431–460.
[55] V.V. Lissianski, W.C. Gardiner, V.M. Zamanski, Combust. Sci. Technol. 111 (1995) 169–183.